

## MIT Open Access Articles

*Thermal conductivity of bulk nanostructured lead telluride*

The MIT Faculty has made this article openly available. **Please share** how this access benefits you. Your story matters.

**Citation:** Hori, Takuma, Gang Chen, and Junichiro Shiomi. "Thermal Conductivity of Bulk Nanostructured Lead Telluride." Appl. Phys. Lett. 104, no. 2 (January 13, 2014): 021915. © 2014 AIP Publishing LLC

**As Published:** <http://dx.doi.org/10.1063/1.4862323>

**Publisher:** American Institute of Physics (AIP)

**Persistent URL:** <http://hdl.handle.net/1721.1/97253>

**Version:** Final published version: final published article, as it appeared in a journal, conference proceedings, or other formally published context

**Terms of Use:** Article is made available in accordance with the publisher's policy and may be subject to US copyright law. Please refer to the publisher's site for terms of use.



# Thermal conductivity of bulk nanostructured lead telluride

Takuma Hori,<sup>1</sup> Gang Chen,<sup>2</sup> and Junichiro Shiomi<sup>1,3,a)</sup>

<sup>1</sup>Department of Mechanical Engineering, The University of Tokyo, Bunkyo, Tokyo 113-8656, Japan

<sup>2</sup>Department of Mechanical Engineering, Massachusetts Institute of Technology, Cambridge, Massachusetts 02139, USA

<sup>3</sup>PRESTO, Japan Science and Technology Agency, Kawaguchi, Saitama 332-0012, Japan

(Received 13 November 2013; accepted 2 January 2014; published online 16 January 2014)

Thermal conductivity of lead telluride with embedded nanoinclusions was studied using Monte Carlo simulations with intrinsic phonon transport properties obtained from first-principles-based lattice dynamics. The nanoinclusion/matrix interfaces were set to completely reflect phonons to model the maximum interface-phonon-scattering scenario. The simulations with the geometrical cross section and volume fraction of the nanoinclusions matched to those of the experiment show that the experiment has already reached the theoretical limit of thermal conductivity. The frequency-dependent analysis further identifies that the thermal conductivity reduction is dominantly attributed to scattering of low frequency phonons and demonstrates mutual adaptability of nanostructuring and local disordering. © 2014 AIP Publishing LLC.

[<http://dx.doi.org/10.1063/1.4862323>]

Lead telluride (PbTe) is a promising thermoelectric material for intermediate temperature (400 K–800 K) applications. This is partially attributed to their intrinsically low lattice thermal conductivity ( $\sim 2 \text{ W m}^{-1} \text{ K}^{-1}$  at room temperature<sup>1</sup>) since the dimensionless figure of merit  $ZT$  is inversely proportional to thermal conductivity. Nanostructuring is a growing practical approach to further reduce lattice thermal conductivity of bulk materials. A general strategy is to scatter phonons by the nanostructure interfaces without appreciably interfering with the charge-carrier transport. A successful form of bulk nanostructured materials has been the sintered nanograins with the nominal grain size smaller and larger than the phonon and charge-carrier mean free paths, respectively.<sup>2</sup> However, the first-principles-based phonon transport calculations of single crystal PbTe indicate that heat is carried mostly by phonons with mean free paths smaller than 10 nm, and the above window of mean free paths does not exist for PbTe.<sup>3,4</sup>

An alternative would be to locally precipitate nanocrystals (nanoinclusions) of different specie inside the PbTe matrix.<sup>5–11</sup> The most successful case to this date is PbTe matrix with strontium telluride (SrTe) nanoinclusions,<sup>8,10</sup> which marked  $ZT = 2.2$  at 800 K with appropriate doping and microstructuring. It has been shown that the lattice thermal conductivity can be reduced without sacrificing the electrical conductivity and Seebeck coefficient, which is attributed to the formation of the coherent interface with seamless bonds between the nanocrystalline precipitates and the matrix (“endotaxial nanostructure”).

To further improve and optimize the PbTe-based bulk nanostructured thermoelectric materials, it is helpful to know the theoretical limit of the lattice thermal conductivity. This gives us insight into how well the nanostructured interfaces have performed to scatter phonons or how further thermal conductivity can be potentially reduced by optimizing the

interfaces. For the sintered nanograins, the lattice thermal conductivity can be estimated by simplifying the picture with a single grain size value. Anharmonic lattice dynamics calculations based on the first-principles<sup>3,4,12–14</sup> give mode-dependent phonon transport properties, from which lattice thermal conductivity reduction can be calculated for extreme scenarios, e.g., trimming the phonon mean free paths longer than the grain size<sup>15</sup> or enforcing the boundary scattering model using Matthiessen’s rule at the Casimir limit.<sup>16</sup> On the other hand, the effect of nanoinclusions is much less evident since the structure is topologically more complicated.

This work aims to identify a theoretical limit of lattice thermal conductivity of PbTe/nanoinclusion materials in the view of phonon gas kinetics. The phonon Boltzmann transport simulation under relaxation time approximation were performed for a PbTe matrix with cubic nanoinclusions. By using the frequency/branch dependent phonon transport properties of single crystal PbTe obtained based on first principles, the simulations realize more accurate representation of the intrinsic phonon transport than the simplified empirical models.<sup>7,8,11</sup> A maximum interface-scattering scenario is realized by making the PbTe-nanoinclusion interface to completely and diffusively reflect phonons (zero transmission probability).

In the view of phonon gas kinetics, the Boltzmann transport equation of phonon distribution function  $f$  under relaxation time approximation is written as

$$\frac{\partial f_s(\omega, \mathbf{r})}{\partial t} + v_s(\omega) \mathbf{e} \cdot \nabla_{\mathbf{r}} f_s(\omega, \mathbf{r}) = -\frac{f_s(\omega, \mathbf{r}) - f_0(\omega, T)}{\tau_s(\omega, T)}, \quad (1)$$

where  $s$ ,  $\omega$ ,  $\mathbf{r}$ ,  $v$ ,  $f_0$ ,  $T$ , and  $\tau$  are the phonon polarization, the frequency, the position, the group velocity, the Bose Einstein distribution, the temperature, and the relaxation time, respectively. In this study, to realize the calculation of the nanostructured geometry, Boltzmann transport equation was solved stochastically using the Monte Carlo method.<sup>17–22</sup>

<sup>a)</sup> Author to whom correspondence should be addressed. Electronic mail: shiomi@photon.t.u-tokyo.ac.jp.

Here, only the longitudinal acoustic (LA) and transverse acoustic (TA) branches are considered since the contributions of optical modes to PbTe lattice thermal conductivity are much smaller than those of acoustic modes.<sup>3</sup> The energy-based variance-reduced Monte Carlo formulation<sup>21</sup> with the effective energy of the phonon particle  $\varepsilon = 8.6 \times 10^{-26}$  J was used to ensure the accuracy and speed of the simulations.

The geometry of a typical simulation cell is shown in Fig. 1, where a cubic nanoinclusion is arranged in the middle of the simulation cell. With the aim to model the maximum interface-scattering scenario, the phonon transmission probability across the PbTe-nanoinclusion interface was set to zero (i.e., complete phonon reflection), and the total diffusive reflection condition was applied using the Lambert's cosine law. Therefore, the nanoinclusion is essentially a nanovoid, in which phonon transport does not need to be considered. This does not only make the simulation simple but also exclude ambiguities in modeling the interface, and thus, in identifying the theoretical limit of lattice thermal conductivity for a given nanoinclusion size and volume fraction. Here, we do not account for the anisotropy in the reflection direction due to the wave scattering characteristics.<sup>23</sup> However, we have confirmed that altering the reflection characteristics from diffusive to specular does not further reduce the lattice thermal conductivity. The length of the nanoinclusion  $a$  is varied from 1 nm to 20 nm. For each value of  $a$ , the dependence of the lattice thermal conductivity on the nanoinclusion volume fraction was studied by varying  $L$ . The scattering cross section here is the geometrical one, and, for simplicity, we do not consider the wave-vector dependent variation of the cross section due to the wave scattering.<sup>24</sup>

The simulation models the steady-state heat conduction through 3-d periodic nanostructures in an infinite domain. This was realized by applying the periodic boundary conditions in the  $y$  and  $z$  directions and the *periodic distortion boundary condition*<sup>20,21</sup> in the  $x$  direction (the heat flow direction). The periodic distortion boundary condition

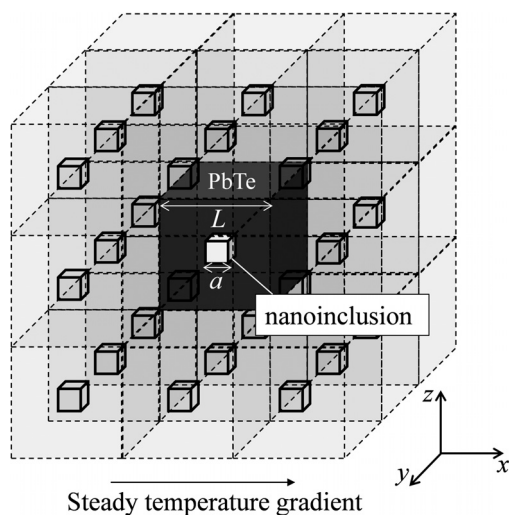


FIG. 1. A schematic of the Monte Carlo simulation cell of phonon transport in PbTe with nanoinclusions. The nanoinclusion is arranged at the center of the simulation cell. The periodic distortion boundary condition<sup>20</sup> is applied in the  $x$  direction and the periodic boundary condition in the  $y$ - $z$  plane.

imposes periodicity only on the distortions of the phonon distribution functions ( $f-f_0$ ), which enables us to assign different temperatures to the left and right virtual boundaries through  $f_0$ .<sup>20,21</sup> Using the boundary conditions, the simulation of a unitary cell allows us to access the properties of steady-state heat conduction through a periodic structure (Fig. 1).

The simulation is initialized by randomly placing phonons in the simulation cell with frequency and polarization distributions that were determined using the density of states and Bose Einstein statistics. Each phonon is initially given a random propagation direction. The simulation cell is divided into subcells to define the local temperatures, which was calculated from their phonon energy. After the initialization, each phonon propagates in specific direction at its group velocity. The phonon group velocity and density of states of a single crystal PbTe were calculated in advance using the harmonic interatomic force constants obtained from first principles.<sup>3</sup> The group velocity was averaged over the first Brillouin zone for each branch to be a function of frequency (Fig. 2).

Within each time step  $\Delta t$ , a phonon may be scattered by other phonons (intrinsic phonon-phonon scattering) or at the interface. Intrinsic phonon scattering occurs with the probability  $P = 1 - \exp(-\Delta t/\tau)$  and resets all the phonon states (frequency, polarization, and propagation direction). The frequency- and temperature-dependent relaxation time of the single crystal PbTe was calculated in advance by Fermi's golden rule of three-phonon scattering processes, using the anharmonic interatomic force constants obtained based on first principles calculations.<sup>3</sup> The results with finite wavevector-space mesh were fitted by the Klemens expression  $C\omega^{-2}$ , where  $C$  is a constant (Fig. 2). The obtained values are  $C = 2.89 \times 10^{14} \text{ s}^{-1}$  and  $1.44 \times 10^{14} \text{ s}^{-1}$  at 300 K and 600 K, respectively.

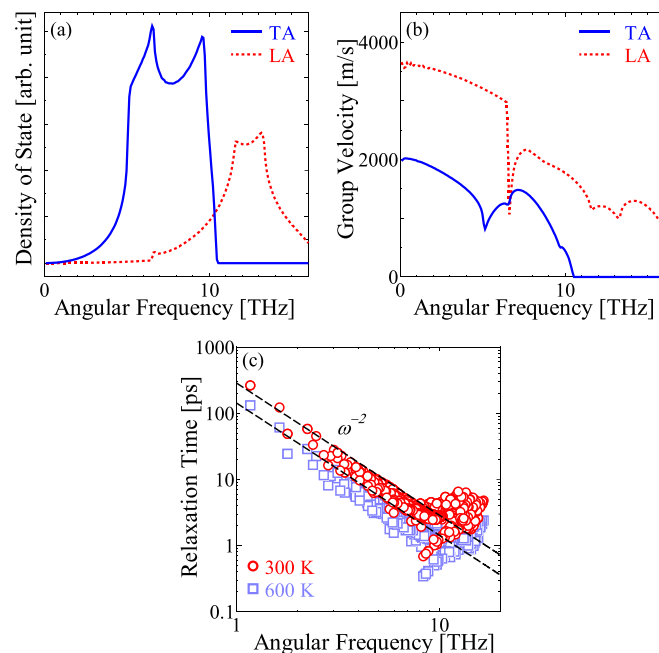


FIG. 2. The frequency- and branch-dependent phonon transport properties, (a) the density of states, (b) group velocity, and (c) relaxation time, obtained from the first-principles based anharmonic lattice dynamics calculations. TA and LA denote the transverse and longitudinal acoustic branches.

The simulations were performed for two different average temperatures 300 K and 600 K. The time step of the simulation is 0.05 ps for both temperatures. The temperature difference between the hot and cold boundaries was set to be  $\Delta T = 0.2$  K. Convergence to a steady-state heat flux with a linear temperature gradient was achieved in 200 000 time steps, and then the data were sampled for another 200 000 time steps to calculate the lattice thermal conductivity. The lattice thermal conductivity was calculated from Fourier's law,  $\kappa_{\text{lat}} = qL/\Delta T$ , where  $q$  and  $L$  are the heat flux and the length of the simulation cell in the  $x$  direction, respectively. The heat flux was calculated to be  $q = \sum \varepsilon l_x/V$ , where  $\varepsilon$  and  $l_x$  are the phonon energy and the start-to-end distance in a unit time period. The lattice thermal conductivity was time-averaged to reduce the statistical noise in the heat flux. For each nanoinclusion size and volume fraction, 6 different simulations were conducted and ensemble-averaged to further enhance the signal to noise ratio. As a result, the statistical uncertainty of the calculated lattice thermal conductivity is less than 1%. Before studying the nanostructures, the calculation scheme was validated for bulk single crystal PbTe, and the obtained thermal conductivity agreed with the analytical solution of the phonon Boltzmann transport equation [Eq. (1)] and did not depend on the cell size ( $3 \text{ nm} < L < 14 \text{ nm}$ ).<sup>25</sup>

In Fig. 3, the calculated lattice thermal conductivity is plotted with respect to the volume fraction of the

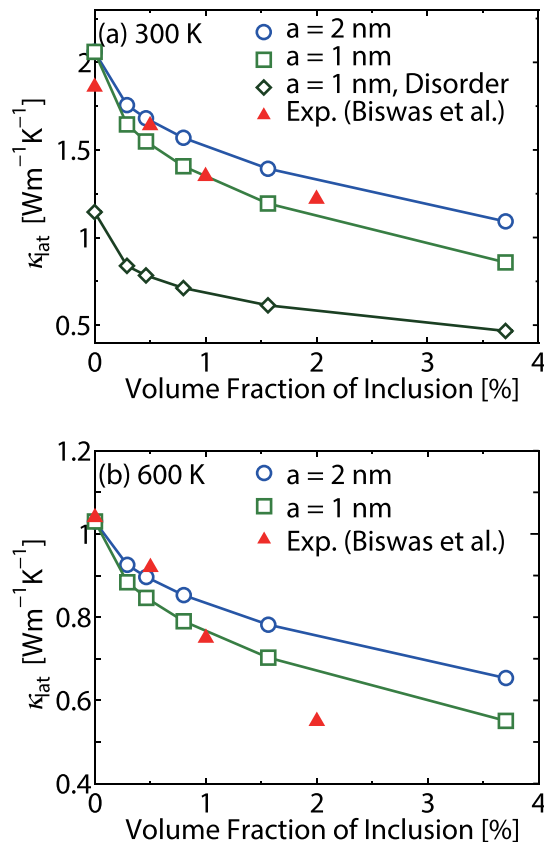


FIG. 3. Nanoinclusion volume-fraction dependence of lattice thermal conductivity  $\kappa_{\text{lat}}$  of the PbTe nanocomposites at (a) 300 K and (b) 600 K. The length of the nanoinclusion  $a$  is set to 1 or 2 nm. The results are compared with the experiments of PbTe/SrTe coherent ("endotaxial") nanocomposites.<sup>8</sup>

nanoinclusion  $a^3/L^3$ . This identifies the minimum thermal conductivity for a given geometrical cross section and volume fraction of the cubic nanoinclusions. For 1 nm nanoinclusions with a realistic volume fraction, thermal conductivity was reduced by about 60%, and the reduction ratio decreases with increasing temperature. Although here we only show the results for a unit cell with one nanoinclusion, we have also performed simulations of random configurations with multiple nanoinclusions per unit cell for the same nanoinclusion size and volume fraction, which made no difference in thermal conductivity as it has been already found in the previous study.<sup>19</sup>

At 300 K, the calculated lattice thermal conductivity in the cases of  $a = 1$  nm and 2 nm agrees well with the measured values of PbTe with SrTe nanoinclusions of the corresponding average size.<sup>8</sup> The agreement indicates that the lattice thermal conductivity in the experiment has reached the theoretical limit of thermal conductivity in view of the phonon gas kinetics. One could argue that some strains, dislocations, and impurities should be present in the PbTe matrix in the experiment, which could also contribute to the reduction of the lattice thermal conductivity. However, adding these effects would result in weaker volume fraction dependence and thus enlarge the discrepancy between the calculation and experiment. Therefore, the agreement in the volume fraction dependence at 300 K suggests validity to assume the pure impurity/defect free PbTe matrix. It should be noted that there still remains uncertainty in the comparison as the lattice thermal conductivity in the experiment at 600 K decreases more sharply with increasing volume fraction than in the corresponding calculation. Nevertheless, the current calculation results suggest that the nanostructure interface in the experiments is extremely effective in inhibiting the phonon transport. This may seem counterintuitive since the PbTe-nanoinclusion interfaces in the experiment was observed to be coherent, however, the coherence could also cause strong residual strain and stress, which may serve as an effective scatterer of phonons.

Figure 4 shows the dependence of the lattice thermal conductivity on the nanoinclusion size ( $a$ ) at 300 K. For all the volume fractions, the dependence becomes stronger as  $a$  decreases, and one-nanometer variation in  $a$  significantly changes the extent of thermal conductivity reduction when  $a$  is smaller than 10 nm, which can be understood from the

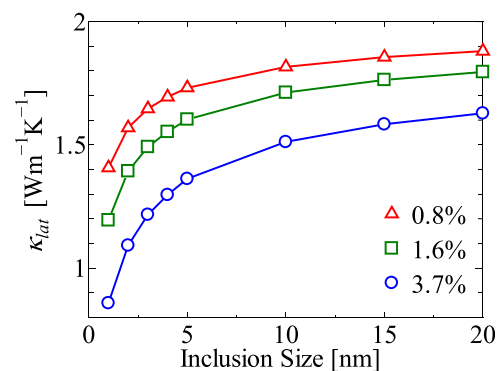


FIG. 4. Nanoinclusion size dependence of the lattice thermal conductivity  $\kappa_{\text{lat}}$  of the PbTe nanocomposites at 300 K for volume fractions 0.8, 1.6, and 3.7%.

mean free path distribution of phonon with noticeable contribution to heat conduction.<sup>3</sup> This indicates the importance of reducing the nanoinclusion size to 1–2 nm as performed in the experiments.<sup>8</sup> The thermal conductivity could be further reduced by making  $a$  even smaller than 1 nm, but one needs to be careful with the limit of the current particle collision picture when  $a$  becomes smaller than the phonon wave packet size. The calculations of the wave characteristics are underway but are not the scope of this work.

The current simulation also enables us to study the microscopic picture of lattice thermal conductivity reduction by the nanoinclusions. To this end, we introduce the frequency dependent lattice thermal conductivity and compare the single crystal and nanostructured material (3.7%,  $a = 1$  nm) at 300 K. Figure 5 shows that the lattice thermal conductivity reduction by the nanoinclusions is mostly attributed to scattering of the low frequency phonons. The high frequency phonons (over 8 THz) are weakly affected because the mean free paths of those phonons are shorter than the nanoinclusion length.

The above frequency-domain analysis suggests that the nanostructuring can be well combined with introducing local disorders (e.g., point defects and impurities), whose phonon scattering rate, in analogy to the Rayleigh scattering, can be roughly approximated to increase as  $\sim \omega^4$ . This is implemented in the Monte Carlo simulations through the relaxation time  $\tau$  using the Matthiessen's rule as  $\tau^{-1} = \tau_{\text{int}}^{-1} + B\omega^4$ , where  $\tau_{\text{int}}$  and  $B$  are the intrinsic phonon relaxation time of PbTe and an empirical constant, respectively. The result shown in Fig. 3(a) was calculated for  $B = 1.0 \times 10^{-40} \text{ s}^3$ , a value that gives the same extent of lattice thermal conductivity reduction as that in the PbTe/PbSe solid solution (40%).<sup>26</sup>

Figure 5 plots the frequency-dependent lattice thermal conductivity by the local-disorder scattering. The figure shows that the presence of the local disorders nearly diminishes the thermal conductivity of phonons in the frequency regime higher than 8 THz without sacrificing the reduction in the low frequency regime caused by the nanoinclusions. This results in a large thermal conductivity reduction in the entire frequency regime, demonstrating the mutual adaptability of nanostructuring and local disordering. As seen in Fig. 5, the

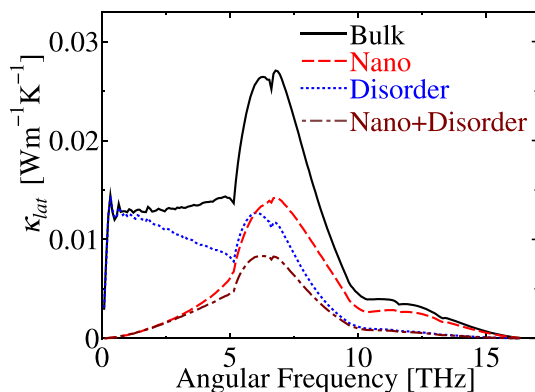


FIG. 5. Frequency dependence of lattice thermal conductivity  $\kappa_{\text{lat}}$  of PbTe nanocomposite at 300 K. The legends “Nano” and “disorder” indicate the PbTe with nanoinclusions (3.7%,  $a = 1$  nm) and local disorders ( $B = 1.0 \times 10^{-40} \text{ s}^3$ ), respectively.

combined approach can reduce the total PbTe lattice thermal conductivity by about 75% in the case of 3.7% nanoinclusions, which is significantly more than the reduction caused solely by nanoinclusions (60%) or by local disorders (40%).

In summary, we have performed the Monte Carlo simulations of Boltzmann phonon transport in PbTe with embedded cubic nanoinclusions using the accurate bulk phonon transport properties obtained from first-principles-based lattice dynamics. The simulations under the maximum interface-phonon-scattering scenario identified the lower-limit lattice thermal conductivity of the nanostructured material in the view of phonon-gas Boltzmann transport. The results suggest that the nanostructure interface in the previous experiments is extremely effective in inhibiting the phonon transport. The frequency domain analysis further identified that the thermal conductivity reduction by the nanoinclusions is mainly caused by scattering of low frequency phonons. This suggests the mutual adaptability with local disordering whose scattering rates increases with phonon frequency. A test case with a realistic alloy concentration shows that the combined approach can significantly reduce thermal conductivity.

This work was partially supported by Research Fellowships of the Japan Society for the Promotion of Science for Young Scientists, Japan Science and Technology Agency, PRESTO, KAKENHI 23760178, the Thermal & Electric Energy Technology Foundation (TH and JS), and by the “Solid State Solar-Thermal Energy Conversion Center (S3TEC),” an Energy Frontier Research Center funded by the U.S. Department of Energy, Office of Science, Office of Basic Energy Sciences under Grant No. DE-SC0001299/DE-FG02-09ER46577 (GC).

<sup>1</sup>I. U. I. Ravich, B. A. Efimova, and I. A. Smirnov, *Semiconducting Lead Chalcogenides* (Plenum Press, New York, 1970).

<sup>2</sup>B. Poudel, Q. Hao, Y. Ma, Y. Lan, A. Minnich, B. Yu, X. Yan, D. Wang, A. Muto, D. Vashaee, X. Chen, J. Liu, M. S. Dresselhaus, G. Chen, and Z. Ren, *Science* **320**(5876), 634–638 (2008).

<sup>3</sup>T. Shiga, J. Shiomi, J. Ma, O. Delaire, T. Radzynski, A. Lusakovski, K. Esfarjani, and G. Chen, *Phys. Rev. B* **85**(15), 155203 (2012).

<sup>4</sup>Z. Tian, J. Garg, K. Esfarjani, T. Shiga, J. Shiomi, and G. Chen, *Phys. Rev. B* **85**(18), 184303 (2012).

<sup>5</sup>K. F. Hsu, S. Loo, F. Guo, W. Chen, J. S. Dyck, C. Uher, T. Hogan, E. K. Polychroniadis, and M. G. Kanatzidis, *Science* **303**(5659), 818–821 (2004).

<sup>6</sup>M. G. Kanatzidis, *Chem. Mater.* **22**(3), 648–659 (2010).

<sup>7</sup>J. Q. He, S. N. Girard, M. G. Kanatzidis, and V. P. Dravid, *Adv. Funct. Mater.* **20**(5), 764–772 (2010).

<sup>8</sup>K. Biswas, J. Q. He, Q. C. Zhang, G. Y. Wang, C. Uher, V. P. Dravid, and M. G. Kanatzidis, *Nat. Chem.* **3**(2), 160–166 (2011).

<sup>9</sup>Y. Z. Pei, J. Lensch-Falk, E. S. Toberer, D. L. Medlin, and G. J. Snyder, *Adv. Funct. Mater.* **21**(2), 241–249 (2011).

<sup>10</sup>K. Biswas, J. He, I. D. Blum, C. I. Wu, T. P. Hogan, D. N. Seidman, V. P. Dravid, and M. G. Kanatzidis, *Nature* **489**(7416), 414–418 (2012).

<sup>11</sup>S.-H. Lo, J. He, K. Biswas, M. G. Kanatzidis, and V. P. Dravid, *Adv. Funct. Mater.* **22**(24), 5175–5184 (2012).

<sup>12</sup>K. Esfarjani and H. T. Stokes, *Phys. Rev. B* **77**(14), 144112 (2008).

<sup>13</sup>K. Esfarjani, G. Chen, and H. T. Stokes, *Phys. Rev. B* **84**(8), 085204 (2011).

<sup>14</sup>J. Shiomi, K. Esfarjani, and G. Chen, *Phys. Rev. B* **84**(10), 104302 (2011).

<sup>15</sup>A. J. Minnich, J. A. Johnson, A. J. Schmidt, K. Esfarjani, M. S. Dresselhaus, K. A. Nelson, and G. Chen, *Phys. Rev. Lett.* **107**(9), 095901 (2011).

<sup>16</sup>F. Yang and C. Dames, *Phys. Rev. B* **87**(3), 035437 (2013).

<sup>17</sup>S. Mazumder and A. Majumdar, *J. Heat Transfer* **123**(4), 749 (2001).



- <sup>18</sup>D. Lacroix, K. Joulain, and D. Lemonnier, *Phys. Rev. B* **72**(6), 064305 (2005).
- <sup>19</sup>M.-S. Jeng, R. Yang, D. Song, and G. Chen, *J. Heat Transfer* **130**(4), 042410 (2008).
- <sup>20</sup>Q. Hao, G. Chen, and M.-S. Jeng, *J. Appl. Phys.* **106**(11), 114321 (2009).
- <sup>21</sup>J.-P. M. Péraud and N. G. Hadjiconstantinou, *Phys. Rev. B* **84**(20), 205331 (2011).
- <sup>22</sup>A. Jain, Y.-J. Yu, and A. J. H. McGaughey, *Phys. Rev. B* **87**(19), 195301 (2013).
- <sup>23</sup>N. Zuckerman and J. R. Lukes, *Phys. Rev. B* **77**(9), 094302 (2008).
- <sup>24</sup>W. Kim and A. Majumdar, *J. Appl. Phys.* **99**(8) 084306 (2006).
- <sup>25</sup>See supplementary material at <http://dx.doi.org/10.1063/1.4862323> for details of the validation.
- <sup>26</sup>H. Wang, A. D. LaLonde, Y. Z. Pei, and G. J. Snyder, *Adv. Funct. Mater.* **23**(12), 1586–1596 (2013).